## Supporting Information

# Robust electrografting on self-organized 3D graphene electrodes.

*Philippe Fortgang,[†] Teddy Tite,[‡] Vincent Barnier[§] Nedjla Zehani,[†] Chiranjeevi Maddi,[‡] Florence Lagarde,[†] Anne-Sophie Loir,[‡] Nicole Jaffrezic-Renault,[†] Christophe Donnet,[‡] Florence Garrelie,[‡*] Carole Chaix[†*]*

[†]Institut des Sciences Analytiques, UMR 5280, CNRS/Université de Lyon 1. 5, rue de la Doua, 69100 Villeurbanne, France. [‡]Université de Lyon, F-69003, Lyon, France, Université de Saint-Étienne, Laboratoire Hubert Curien (UMR 5516 CNRS), 42000 Saint-Étienne, France. [§]Laboratoire Georges Friedel, Ecole Nationale Supérieure des Mines, 42023 Saint-Etienne, France

[*]Corresponding authors: carole.chaix-bauvais@univ-lyon1.fr, florence.garrelie@univ-st-etienne.fr.

## Characterization of the bare self-organized 3D electrodes.

The texturing of the multilayer-graphene is explained through a diffusion of Ni atoms into the Si substrate during the heating. This is clearly evidenced by the presence of vibrational bands at low frequencies (Figure S1a), which was attributed to the formation of silicon-rich nickel-silicides compounds.[1-2] The sharpness of the Raman peaks suggests that the silicides formed are well crystallized. Figure S1b shows the atomic concentration ratio profile of Ni/Si extracted from the Auger electron spectroscopy depth profile measured in the region where the diffusion of Ni atoms into Si substrate occurs. The depth profile is built up by the measurement of the intensity of recorded peaks versus etching time. The first 1500s of etching depicted in Figure S1b corresponds to the graphene top surface. At higher etching time, the Ni/Si ratio increases to reach 1.5 from about 5000 s to 25000 s of etching, which is consistent with the stoichiometry of the stable orthorhombic $Ni_3Si_2$ phase. From thickness measurements performed after etching, 25000 s corresponds to about 150 nm, consistent with the initial thickness of the nickel film.

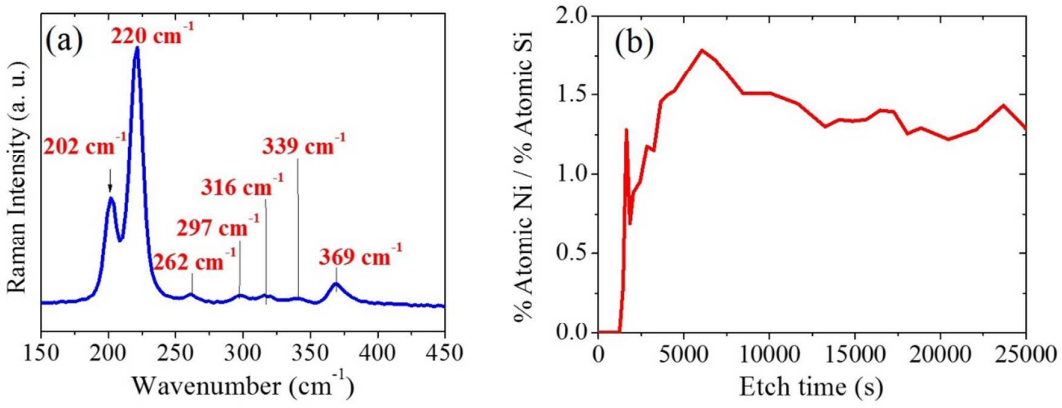


**Figure S1: (a) Raman spectra at low wavenumbers (excitation wavelength of 633 nm). (b) Depth profile of the atomic concentration ratio between Ni and Si derived from Auger spectroscopy.**

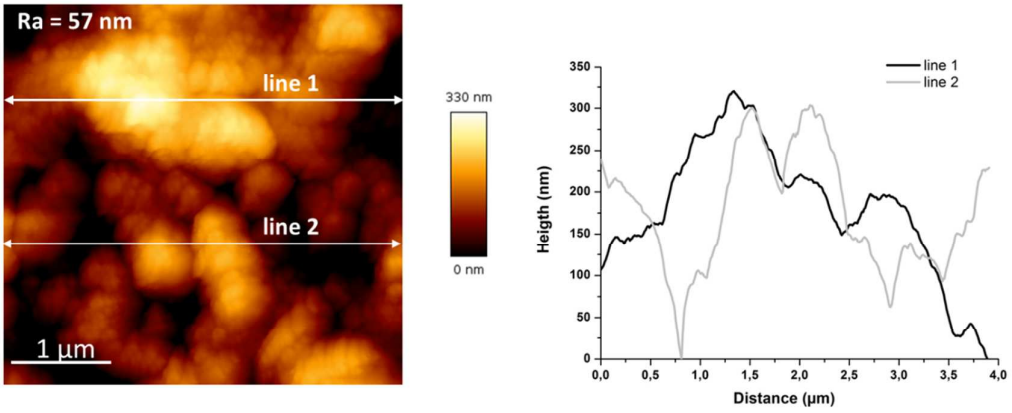


**Figure S2: AFM images of self-organized 3D graphene electrodes. The roughness deduced from Gwyddion analysis is about 57 nm.**

| v in V $s^{-1}$ | $i_{pa}$ in µA | $i_{pc}$ in µA | $E_{pa}$ in V *vs* ECS | $E_{pr}$ in V *vs* ECS | $E_{1/2}$ in V *vs* ECS | $\Delta E_p$ in V |
|---|---|---|---|---|---|---|
| 0.005 | 1.25 | 1.26 | 0.499 | 0.440 | 0.470 | 0.059 |
| 0.01 | 1.86 | 1.83 | 0.499 | 0.440 | 0.470 | 0.059 |
| 0.02 | 2.71 | 2.71 | 0.500 | 0.441 | 0.471 | 0.059 |
| 0.05 | 4.49 | 4.34 | 0.505 | 0.440 | 0.473 | 0.065 |
| 0.1 | 6.51 | 6.15 | 0.505 | 0.438 | 0.472 | 0.067 |
| 0.2 | 9.47 | 9.03 | 0.512 | 0.434 | 0.473 | 0.078 |
| 0.5 | 15.4 | 14.7 | 0.520 | 0.431 | 0.476 | 0.089 |
| 0.8 | 20.1 | 18.7 | 0.531 | 0.431 | 0.481 | 0.100 |
| 1.0 | 22.5 | 21.2 | 0.539 | 0.420 | 0.480 | 0.119 |

**Table S1. Electrochemical characterization of bare 3D graphene by cyclic voltammetry at different scan rates using 0.5 mM ferrocene dimethanol redox probe in 0.1 M $NaClO_4$ aqueous solution.**

## Nicholson Method for k° determination in diffusive system.

A quasi reversible electron transfer process results in a peak-to-peak separation ($\Delta E_p$) that increases with the scan rate ($v$) and this effect allows one to calculate a heterogeneous electron transfer rate (k°) using the commonly used Nicholson method[3] :

$$\psi = k^\circ \left(\frac{D_O}{D_R}\right)^{\alpha/2} \sqrt{\frac{RT}{\pi n F D_O v}} \qquad \text{(eq. S1)}$$

where $\psi$ is the dimensionless kinetic parameter determined from $\Delta E_p$, α the electron transfer coefficient, n the number of electrons transferred during the redox event, $D_O$ and $D_R$ are respectively the diffusion coefficient of the oxidized and reduced forms of the redox mediator, F the Faraday constant, R the gas constant value and T the temperature. In the case of ferrocene redox probe, $D_O$ and $D_R$ are assumed to be equal and that the reduction and the oxidation kinetics are symmetrical, i.e., $\alpha \approx 0.5$ so that eq. S1 can be simplified to

$$\psi = k^\circ \sqrt{\frac{RT}{\pi n F D v}} \qquad \text{(eq. S2)}$$

$\psi$ is calculated using an empirically determined working function[4] for a given $\Delta E_p$:

$$\psi = \frac{(-0.6288 + 0.0021 n \Delta E_p)}{(1 - 0.017 n \Delta E_p)} \qquad \text{(eq. S3)}$$

where $\Delta E_p$ is given in mV and limited to values below ca. 220mV.

| v in V/s | $\Delta E_p$ in mV | $\psi$ |
|---|---|---|
| 0.05 | 65 | 4.689 |
| 0.1 | 67 | 3.512 |
| 0.2 | 78 | 1.426 |
| 0.5 | 89 | 0.861 |
| 0.8 | 100 | 0.598 |
| 1 | 119 | 0.370 |

**Table S2. Empirically determined value of $\psi$ calculated from $\Delta E_p$ value beyond 59mV (quasi-reversible behavior).**

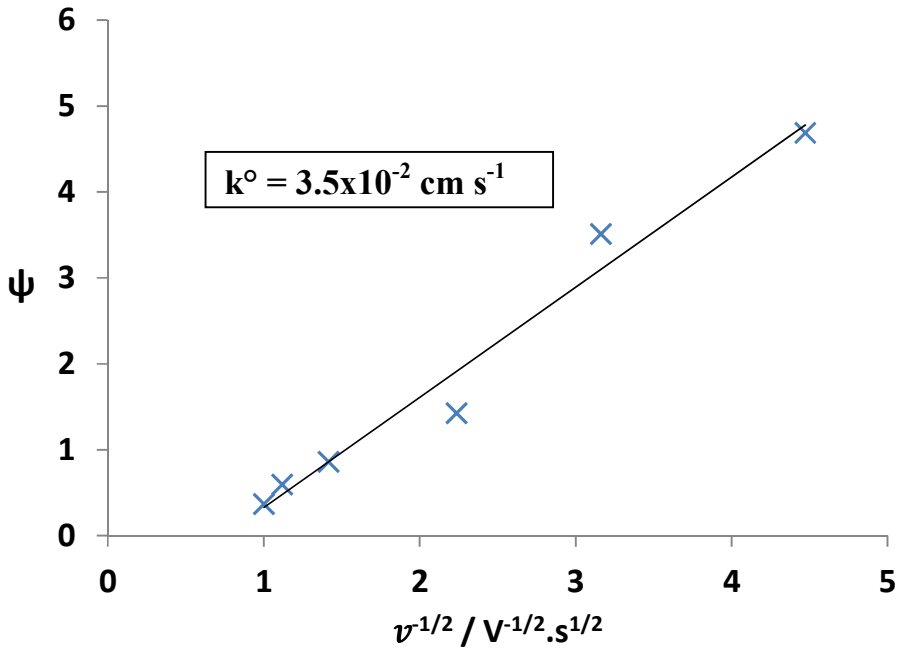


**Figure S3. Variation of $\psi$ with the scan rate using for k° determination from the slope of the $\psi = f(v^{-\frac{1}{2}})$ dependence.**

**Electrochemical grafting of 4-ethynylaniline on self-organized 3D graphene electrodes.**

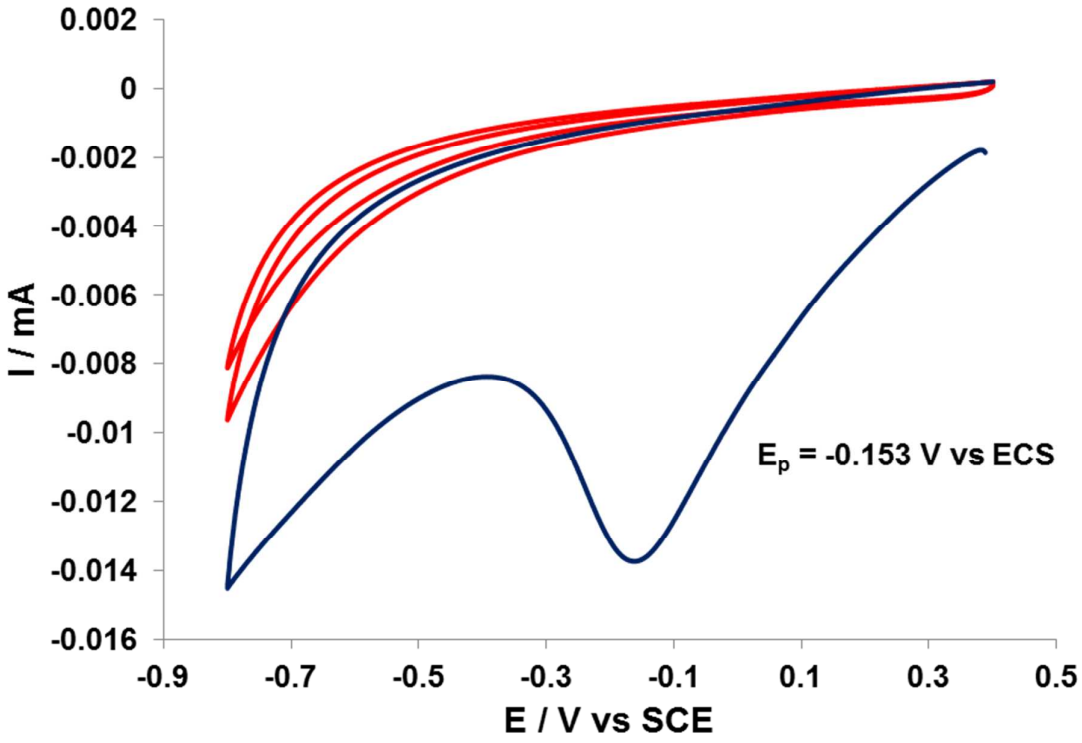


**Figure S4. Voltammogram of the *in-situ* generated 4-ethynylphenyl layer on graphene electrodes at 0.1V/s in 0.1M HCl 40 mM $NaNO_2$ and 2 mM 4-ethynylaniline. The solution was degased with $N_2$ and the reaction was carried out at 4°C. In blue are shown the first CV scan, than in red the two consecutive scans.**

## Laviron analysis for $k_{ET}$ determination in diffusionless electrochemical systems.

The electron transfer rate constant ($k_{ET}$) was calculated with a classical Laviron analysis[5],

$$E_{pc} = E^{\circ\prime} - \frac{RT}{\alpha nF}\ln\left(\frac{\alpha nFv}{RTk_{ET}}\right). \quad \text{(Eq. S4)}$$

$$E_{pa} = E^{\circ\prime} - \frac{RT}{(1-\alpha)nF}\ln\left(\frac{(1-\alpha)nFv}{RTk_{ET}}\right) \quad \text{(Eq. S5).}$$

It consists in recording cyclic voltammograms at different scan rates (υ) and plotting of the relative peak potentials $E^{\circ\prime}$ - $E_p$ versus ln($v$). $E^{\circ\prime}$ is the formal potential and $E_p$ is either the cathodic or the anodic peak potential. We assumed that the electron transfer coefficient ($\alpha$) value is 0.5. The electron transfer rate constant, $k_{ET}$, can be derived from the analysis of the linear part of the plot at the higher scan rates (see Figure S5),

$$k_{ET} = \frac{\alpha nF}{RT}\exp\left(-\frac{intercept}{slope}\right) \quad \text{(Eq. S6).}$$

A $k_{ET}$ of 0.4 $s^{-1}$ was determined.

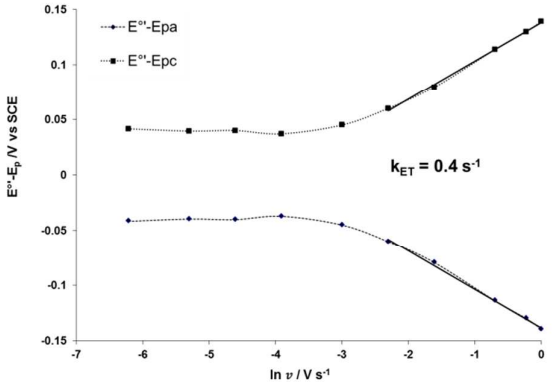


**Figure S5. Plot of $E^{\circ\prime}$ - $E_p$ versus ln($v$). Values at high scan rates (plain lines) are used for $k_{ET}$ determination by Laviron's analysis.**

## Stability of the ferrocene modified 3D graphene electrode.

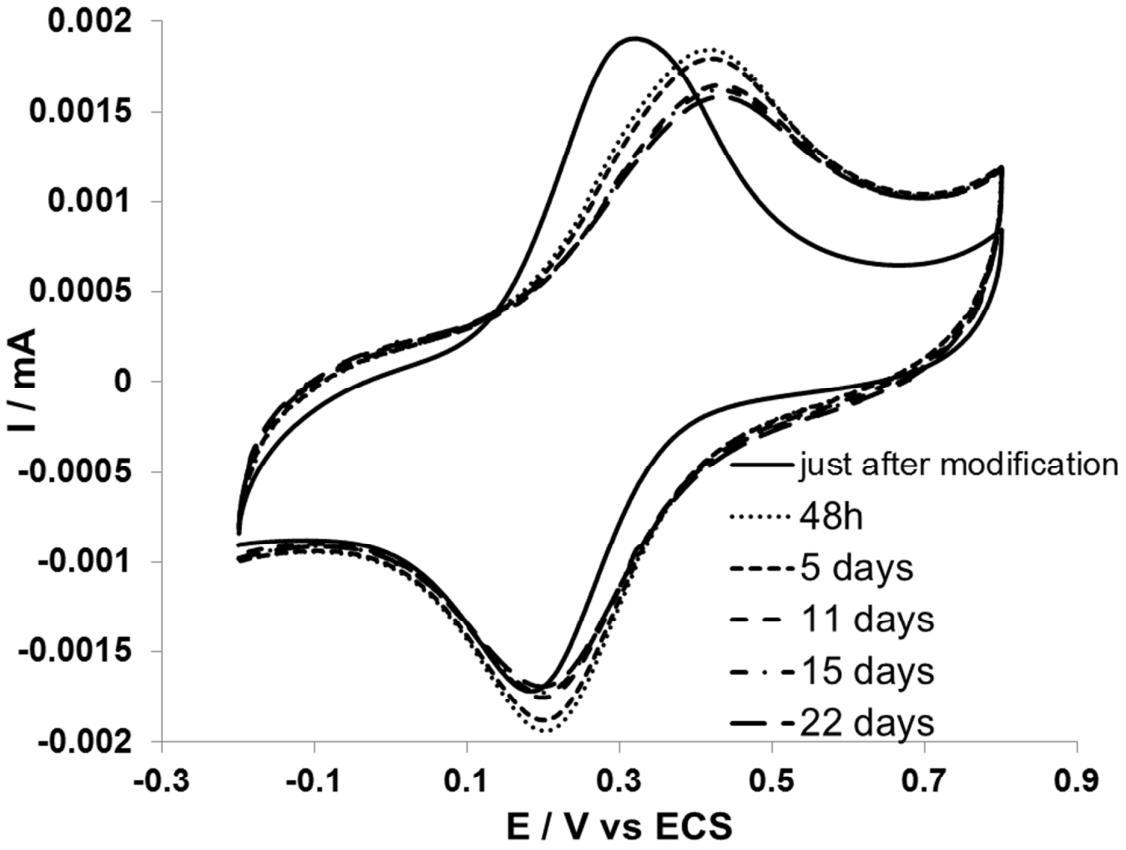


**Figure S6. Voltammograms at 0.1 V $s^{-1}$ in 0.1 M $NaClO_4$ of ferrocene modified 3D graphene electrode. The electrode was kept between each measurement in 0.1M $NaClO_4$ at ambient temperature.**

Voltammograms shown in Figure S6 were used to draw Figure S7. The surface coverage of ferrocene on the graphene modified electrode was electrochemically determined by integration of oxidation and reduction peaks and plotted against time, after the click reaction of Fc-Azide with the 4-ethynylphenyl moieties grafted on graphene.

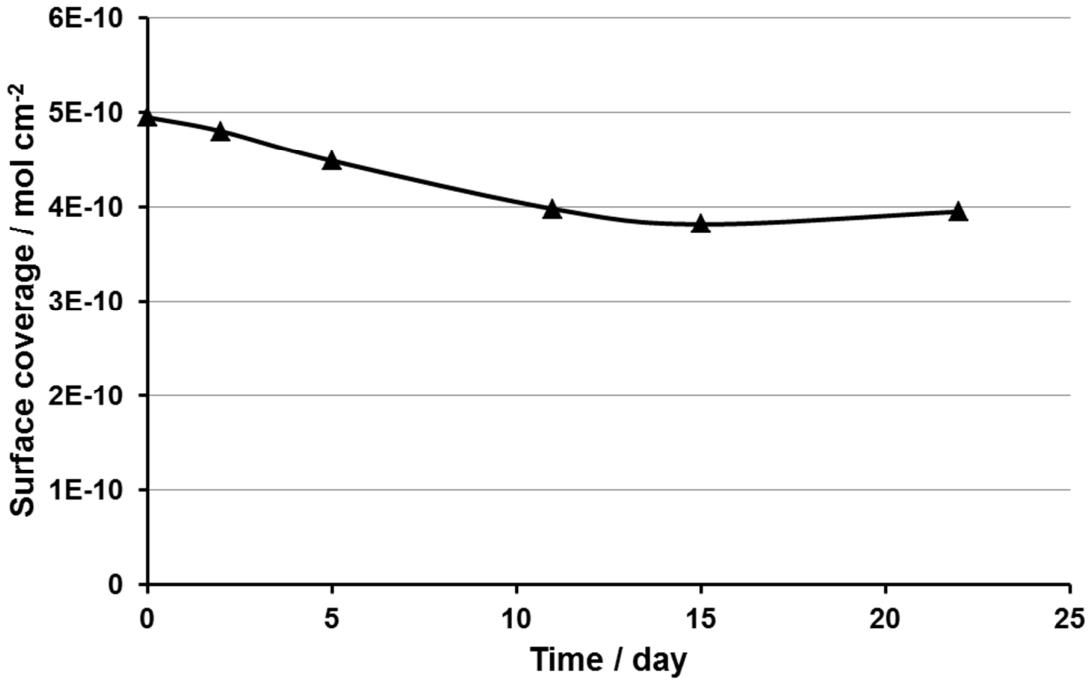


**Figure S7. Electrochemically determined coverage of clicked ferrocene at modified graphene electrodes over time in order to show the stability of the ferrocene functionalized self-organized 3D Graphene.**

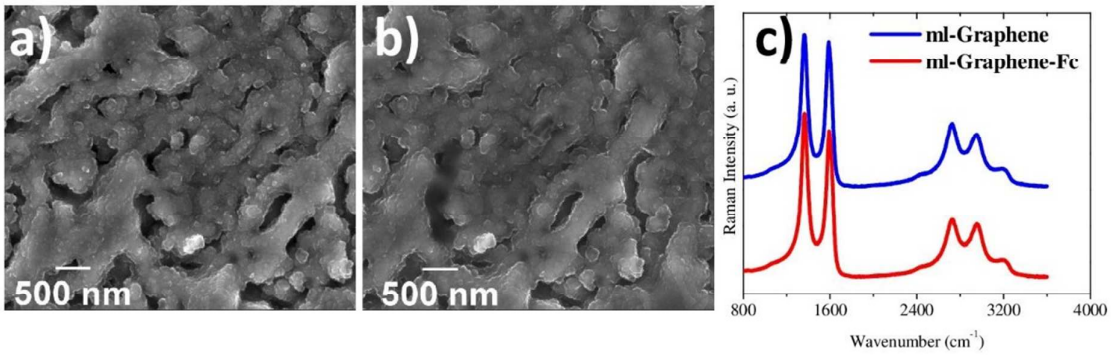


**Figure S8. Scanning electron microscopy images of self-organized 3D graphene before (a) and after (b) electrografting. No structural modification of the graphene induced by the electrografting is evidenced by Raman spectroscopy (c).**

## High energy resolution spectra of Fe2p peak.

To confirm the electrochemical grafting of the graphene-based substrate, further analysis of high energy resolution Fe2p peak was performed (Figure S9) in order to check the signature of ferrocene complex. Three contributions are considered to model the experimental Fe2p spectrum. The first contribution takes into account the Cu LMM Auger transitions which interfere with the Fe2p peak due to the presence of residual trace of catalyst which is highlighted in the Figure 7 with the line-scan of the $Cu2p_{3/2}$ peak intensity. The shape of these Auger transitions was modeled using a set of four peaks consisting of Gaussian-Lorentzian product with a mixing ratio of 30%. The full width at half maximum height of each components as well as the relative areas and positions between the peaks were determined using the Cu LMM spectrum of a pure standard of copper. These parameters were then kept fixed in order to fit the total area of the Cu LMM Auger transitions interfering with the Fe2p peak without changing the shape of these transitions. The two other contributions take into account the oxidation state $Fe^{2+}$ and $Fe^{3+}$ of the Fe moiety in the ferrocene molecule. In the case of oxidation state $Fe^{3+}$, the $2p_{3/2}$ and $2p_{1/2}$ peaks are broadened due to spin-orbit coupling between the $2p_{3/2}$ and $2p_{1/2}$ core holes and the unpaired 3d electrons which induces multiplet components.[6] Moreover, in addition to multiplet structures, shake-up satellite structures associated with $2p_{3/2}$ and $2p_{1/2}$ appear due to the movement of an electron from 3d orbital to the empty 4s orbital during ejection of the core 2p electron.[7] The typical energy resolution of the spectrometer does not allow to see discrete peaks due to multiplet splitting effect which is observed in the spectrum as the asymmetric broadening of the 2p peaks. These peaks were then modeled using Gaussian-Lorentzian product functions associated with a tail composed of a mix of a constant tail height and exponential tail height[8] whilst simple Gaussian-Lorentzian product functions with a mixing ratio of 30% were used for the shake-up satellites. The same line-shapes either from the principal peak or for the satellite peak were used for $2p_{1/2}$ and $2p_{3/2}$

peaks with an area ratio of 0.5. For the oxidation state $Fe^{2+}$, the strong crystal field splitting in the ferrocene force the $Fe^{2+}$ cation to have a low spin. For low spin $Fe^{2+}$, the $2p_{3/2}$ and $2p_{1/2}$ peaks show no multiplet and shake-up structures because all six 3d electrons are spin paired[9] and these two peaks are consequently not broadened and symmetric compared to the $Fe^{3+}$ cation. These peaks were modeled with a Gaussian-Lorentzian product functions with a mixing ratio of 30%.

The Figure S9a shows the Fe2p spectrum of the 2-azidoethyl ferrocene moiety physisorbed on a silicon wafer. The experimental spectrum was fitted using $Fe^{2+}$ and $Fe^{3+}$ components with line-shapes described above. Binding energies of $Fe2p_{3/2}$ and $Fe2p_{1/2}$ doublet for $Fe^{2+}$: 707.9 eV and 720.8 eV and for $Fe^{3+}$: 711.5 eV and 724 eV are consistent with literature findings.[10-12] The $Fe^{2+}$ oxidation state is largely predominant with a $Fe^{2+}/Fe^{3+}$ atomic ratio of 3.34. The same spectrum was carried out on the graphene-based sample electrochemical grafted with ferrocene derivative (Figure S9b). The functions used to model $Fe^{2+}$ and $Fe^{3+}$ components were the same than for the reference spectrum on Fc-Azide and the experimental spectrum was fitted taking into account also the contribution of Auger Cu transitions. The binding energies of $Fe2p_{3/2}$ and $Fe2p_{1/2}$ doublet found for $Fe^{2+}$: 707.8 eV and 720.7 eV and for $Fe^{3+}$: 711.3 eV and 723.9 eV are close to those found for the reference. The multiplet and shake-up satellite structures are clearly visible for the $Fe^{3+}$ component. Moreover, looking at the $Fe2p_{3/2}$ doublet, it can be noticed that the energy separation and relative intensity of satellite to main peak avoid the assignment to iron oxide[9] which allows excluding a possible decomplexation of the ferrocene moieties. As compared to the reference (Figure S9a), the $Fe^{2+}/Fe^{3+}$ atomic ratio drops to 0.45. According to Zheng *et al.*,[13] switching of oxidation state can be the result of the exposition of ferrocene molecules to X-rays but this irradiation tends to reduce $Fe^{3+}$ to $Fe^{2+}$. Moreover the proportion of $Fe^{3+}$ is weak for the Fc-Azide moieties physisorbed (Figure S9a) which was analysis in the same condition. Following Zanoni *et al.*,[10] another explanation

of the increase of $Fe^{3+}$ surface concentration at the expenses of $Fe^{2+}$ is an effect of electrochemical ageing which can be found at increasing number of voltammetric cycles. In particular the authors have shown that the oxidation state $Fe^{3+}$ was originated from the substrate-assisted redox process where the overall +1 charge of the surface complex is neutralized by the presence of surface $O^-$ groups.

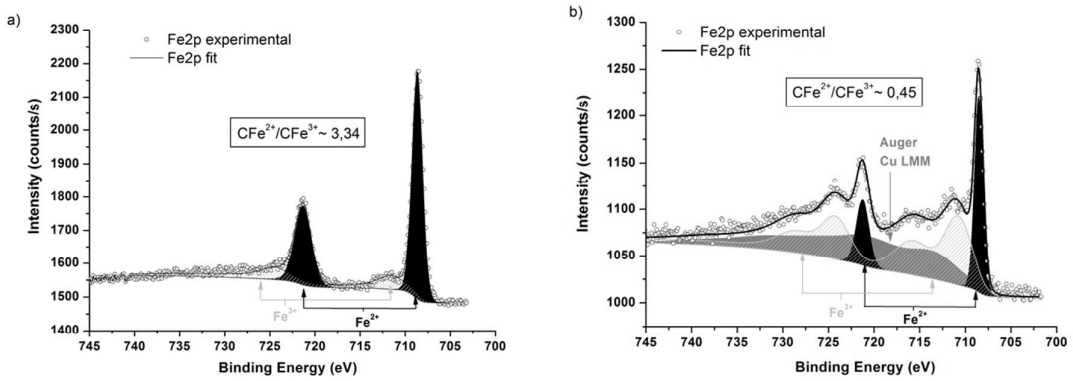


**Figure S9. High energy resolution spectra of Fe2p peak for: a) Fc-Azide moieties physisorbed on a silicon wafer and b) Ferrocene functionalized 3D graphene. The experimental spectrum (open circles) are fitted using components associated to $Fe^{3+}$ and $Fe^{2+}$ oxidation states in the ferrocene complex and components corresponding to Cu LMM Auger transitions for the graphene-based sample due to residual traces of Cu catalyst.**

## XPS inelastic electron background analysis of the in-depth distribution of nitrogen

The analysis was performed using the "analyse" QUASES software package developed by Tougaard.[14] Details of the formalism used for surface quantitative analysis from the shape of recorded spectrum can be found in the literature.[15] The basic principle can be briefly summarized as follow. Due to multiple inelastic scattering events, electrons lose energy during their travel through the solid which means that the shape of the measured spectrum on a wide energy range (~ 100 eV) is associated to a differential inelastic cross section and strongly dependent to the in-depth distribution of the emitters. Tougaard showed that the atomic spectrum F(E) can be extracted from the measured spectrum J(E) using the following formalism:

$$F(E) = \frac{1}{P_1}\left\{J(E) - \int dE' J(E) \int_{-\infty}^{+\infty} ds \exp(i2\pi s(E-E'))\left(1 - \frac{P_1}{P(s)}\right)\right\} \qquad \text{(Eq. S7)}$$

where

$$P_1 = \int_0^{\infty} dz f(z) \exp\left(\frac{-z}{\lambda cos\theta}\right) \text{ and } P(s) = \int_0^{\infty} dz f(z) \exp\left(\frac{-z}{\lambda cos\theta}\left[1 - \int_0^{\infty} dT\, \lambda K(T) \exp(-isT\right]\right)$$

With E the kinetic energy, K(T) the differential inelastic cross section, λ the inelastic mean free path, θ the angle between surface normal and detector and f(z) the in-depth profile. Using these equations, for a specific depth profile f(z), the shape and the intensity of F(E) can be calculated from J(E). The corrected spectrum is then compared to F(E) for a reference sample with homogeneous known distribution. The profile f(z) is then determined after several iterations until the corrected spectrum matches the intrinsic spectrum of the reference sample. The model chosen for the depth distribution of nitrogen is a buried layer for which we try to estimate the thickness and the depth of burying. A value of 2.8 nm was chosen for λ of an electron coming from N1s level and travelling through a layer of ferrocene according to

calculation using TPP2m equation.[16] Universal cross section[17] with C=1643 $eV^2$ and B=3000 $eV^2$ was used for approximation of K(T) following the expression:

$$\lambda K(T) = \frac{BT}{(C+T^2)^2} \quad \text{(Eq. S8)}$$

Finally, a CN film with homogenous nitrogen depth distribution prepared using pulsed laser deposition was chosen as reference sample.

**References**:


(1) Bhaskaran, M.; Sriram, S.; Perova, T. S.; Ermakov, V.; Thorogood, G. J.; Short, K. T.; Holland, A. S., In-situ Micro-Raman Analysis and X-ray Diffraction of Nickel Silicide Thin Films on Silicon. *Micron* **2009,** *40* (1), 89-93.

(2) Li, F.; Yue, H.; Wang, P.; Yang, Z.; Wang, D.; Liu, D.; Qiao, L.; He, D., Synthesis of Core-Shell Architectures of Silicon Coated on Controllable Grown Ni-Silicide Nanostructures and their Lithium-Ion Battery Application. *CrystEngComm* **2013,** *15* (36), 7298-7306.

(3) Nicholson, R. S., Theory and Application of Cyclic Voltammetry for Measurement of Electrode Reaction Kinetics. *Anal. Chem.* **1965,** *37* (11), 1351-1355.

(4) Lavagnini, I.; Antiochia, R.; Magno, F., An Extended Method for the Practical Evaluation of the Standard Rate Constant from Cyclic Voltammetric Data. *Electroanalysis* **2004,** *16* (6), 505-506.

(5) Laviron, E., General Expression of the Linear Potential Sweep Voltammogram in the Case of Diffusionless Electrochemical Systems. *J. Electroanal. Chem. Interfacial Electrochem.* **1979,** *101* (1), 19-28.

(6) Gupta, R. P.; Sen, S. K., Calculation of Multiplet Structure of Core p-Vacancy Levels. *Physical Review B* **1974,** *10* (1), 71-77.

(7) Yin, L.; Adler, I.; Tsang, T.; Matienzo, L. J.; Grim, S. O., Paramagnetism and Shake-Up Satellites in X-Ray Photoelectron Spectra. *Chemical Physics Letters* **1974,** *24* (1), 81-84.

(8) Briggs, D.; Seah, P., *Practical Surface Analysis: Auger and X-Ray Photoelectron Spectroscopy*. Wiley: **1990**.

(9) Grosvenor, A. P.; Kobe, B. A.; Biesinger, M. C.; McIntyre, N. S., Investigation of Multiplet Splitting of Fe 2p XPS Spectra and Bonding in Iron Compounds. *Surf. Interface Anal.* **2004,** *36* (12), 1564-1574.

(10) Zanoni, R.; Cattaruzza, F.; Coluzza, C.; Dalchiele, E. A.; Decker, F.; Di Santo, G.; Flamini, A.; Funari, L.; Marrani, A. G., An AFM, XPS and Electrochemical Study of Molecular Electroactive Monolayers Formed by Wet Chemistry Functionalization of H-terminated Si(100) with Vinylferrocene. *Surf. Sci.* **2005,** *575* (3), 260-272.

(11) Umaña, M.; Rolison, D. R.; Nowak, R.; Daum, P.; Murray, R. W., X-Ray Photoelectron Spectroscopy of Metal, Metal Oxide, and Carbon Electrode Surfaces Chemically Modified with Ferrocene and Ferricenium. *Surf. Sci.* **1980,** *101* (1–3), 295-309.

(12) Polzonetti, G.; Faruffini, V.; Furlani, A.; Russo, M. V., X-Ray Photoelectron Spectroscopy of Iodine-doped Polyethynylferrocene. *Synthetic Metals* **1988,** *25* (4), 375-384.

(13) Zheng, F.; Pérez-Dieste, V.; McChesney, J. L.; Luk, Y.-Y.; Abbott, N. L.; Himpsel, F. J., Detection and Switching of the Oxidation State of Fe in a Self-assembled Monolayer. *Surf. Sci.* **2005,** *587* (3), L191-L196.
(14) Tougaard, S., Accuracy of the Non-Destructive Surface Nanostructure Quantification Technique Based on Analysis of the XPS or AES Peak Shape. *Surf. Interface Anal.* **1998,** *26* (4), 249-269.
(15) Tougaard, S., Practical Algorithm for Background Subtraction. *Surf. Sci.* **1989,** *216* (3), 343-360.
(16) Tanuma, S.; Powell, C. J.; Penn, D. R., Calculations of Electron Inelastic Mean Free Paths. V. Data for 14 Organic Compounds over the 50–2000 eV Range. *Surf. Interface Anal.* **1994,** *21* (3), 165-176.
(17) Tougaard, S., Universality Classes of Inelastic Electron Scattering Cross-sections. *Surf. Interface Anal.* **1997,** *25* (3), 137-154.